Dynamic Time Switching for MIMO Wireless Information and Power Transfer

Seowoo Kang, Hoon Lee, *Member, IEEE*, Seokju Jang, *Student Member, IEEE*, Hanjin Kim, *Student Member, IEEE*, and Inkyu Lee, *Fellow, IEEE*

***Abstract*— This paper studies simultaneous wireless information and power transfer (SWIPT) techniques for point-to-point multiple-input multiple-output channels, where a multi-antenna transmitter conveys information and energy at the same time to a multi-antenna receiver equipped with time switching (TS) circuits for an energy harvesting (EH) mode and an information decoding (ID) mode. Unlike conventional uniform TS (UTS) structure where all the receive antennas at the receiver employ a single TS circuit, in this paper, we propose a general dynamic TS (DTS) receiver architecture which has an individual TS circuit for each antenna. In the proposed DTS, the operation modes of the antennas can be dynamically changed to improve SWIPT performance. We aim to identify the achievable rate–energy (R–E) tradeoff of the DTS protocol for both linear and non-linear EH models by maximizing the information rate subject to the EH constraint. This results in joint optimization of the transmit covariance matrices and the time durations for the EH and the ID modes of the receive antennas, which is jointly non-convex in general. To tackle the non-convexity of the original problem, the successive convex approximation technique is adopted by addressing a series of approximated convex problems. As a result, efficient optimization algorithms are proposed for determining the boundary points of the achievable R–E region. We also provide a low-complexity algorithm which achieves near-optimal performance with much reduced complexity. Numerical results demonstrate that the proposed DTS presents significant performance gains over conventional UTS approaches.**

***Index Terms*— Wireless information and power transfer, MIMO, time switching, rate-energy region.**

I. Introduction

RECENTLY, wireless energy transfer (WET) techniques exploiting radio frequency (RF) signals have received much attention thanks to its capability of supplying power to energy-demanding devices without replacing their batteries [1]–[3]. Combining the WET with traditional wireless communication systems, simultaneous wireless information and power transfer (SWIPT), which sends information and energy at the same time over the same frequency band, has been intensively studied in [4]–[18].

The most challenging issue for designing the SWIPT system is that the information and the energy cannot be extracted by the same circuit module due to hardware limitations [4]. To tackle this difficulty, two practical SWIPT receiver structures, power splitting (PS) and time switching (TS) receivers, have been investigated [7]–[14]. In the PS method, the receiver divides the received signal into an ID part and an EH part with different power ratio [7]–[11]. In [4] and [11], non-trivial rate-energy (R-E) regions were analyzed when the same PS ratio is employed across all the antennas. These works were extended in [9] and [10] to a general case where the PS factors are different for each antenna.

In contrast to the PS-based systems, the TS receiver changes its operation between the ID and the EH modes in the time domain. To improve the SWIPT performance, the time durations for the two modes at the receiver as well as the precoding matrices at the transmitter should be carefully optimized, which results in totally different problem formulations compared to the PS method. The TS receiver has received attention in recent researches, since it is practically easier to implement than the PS circuit structure [11]–[18].

Zhang and Ho [4] studied the SWIPT system in point-to-point (P2P) multiple-input multiple-output (MIMO) channels. Assuming that the identical TS ratio is applied to all the receive antennas, the optimal R-E tradeoff curve was identified. In [12], energy-efficient resource allocation algorithms were presented for the P2P SWIPT systems with a TS receiver. The work in [13] analyzed the robust outage R-E regions in the TS approach with imperfect channel state information (CSI). The TS-based SWIPT methods have also been applied to relay systems [15], [16], multi-user broadcast channels [14], [17], and multi-cell networks [11], [18]. A transmit TS scheme was proposed for multi-cell SWIPT systems in [19] which splits the beamforming vectors for the EH and the ID operations.

All the works mentioned above adopted a linear EH model where the relation between the input RF signal power and the output harvested direct current (DC) power is assumed to be linear. Although the linear EH model is simple, it would not be easy to capture non-linear characteristics of practical diodes especially when the input RF power is large [1], [20].

Manuscript received October 10, 2018; revised January 9, 2019; accepted February 4, 2019. Date of publication February 15, 2019; date of current version June 14, 2019. This work was supported by the National Research Foundation (NRF) through the Ministry of Science, ICT and Future Planning, Korean Government, under Grant 2017R1A2B3012316. The associate editor coordinating the review of this paper and approving it for publication was I. Krikidis. *(Corresponding author: Inkyu Lee.)*

S. Kang, S. Jang, H. Kim, and I. Lee are with the School of Electrical Engineering, Korea University, Seoul 02841, South Korea (e-mail: kangsw1215@korea.ac.kr; seokju@korea.ac.kr; hanjin8612@korea.ac.kr; inkyu@korea.ac.kr).

H. Lee is with the Department of Information and Communications Engineering, Pukyong National University, Busan 48513, South Korea (e-mail: hlee@pknu.ac.kr).

Color versions of one or more of the figures in this paper are available online at http://ieeexplore.ieee.org.

Digital Object Identifier 10.1109/TCOMM.2019.2899605

To characterize this nature, a piecewise linear approximation was employed in [21] for modeling non-linearity of the practical EH circuitry. An analytical non-linear EH model was introduced in [22] by fitting logistic functions over real measurement data. Based on this result, Jiang *et al.* [23] studied the EH system with the PS receiver. Xiong *et al.* [24] examined the performance of the TS architecture in the MIMO systems and presented an iterative algorithm which determines the achievable R-E region under the non-linear logistic function model.

On the other hand, existing works on the TS-based SWIPT systems have implicity assumed that the receiver is equipped with a single TS circuit. In such *uniform TS (UTS)* approaches, the receiver can only operate either in the ID mode or the EH mode at a given time instant. To enhance the SWIPT performance, this paper proposes a new *dynamic TS (DTS)* protocol for P2P MIMO SWIPT systems where each receive antenna at the receiver adopts an individual TS circuit. In the DTS approach, we can separately switch the role of each antenna between the ID mode and the EH mode, and thus, the conventional UTS can be regarded as a special case of the proposed DTS protocol. As the modes of the receive antennas are different, there exist multiple operation phases in the DTS protocol. Hence, the optimization problem in the DTS is more complicated than that for the conventional UTS scheme which only consists of two operation phases.

In this paper, we aim to investigate the fundamental tradeoff between the information rate and the harvested energy both for the linear and non-linear EH models. To this end, we formulate the rate maximization problems subject to the EH constraint as well as the average and peak power budgets at a transmitter, and then perform joint optimization of the transmit covariance matrices at the transmitter and the time durations for the multiple phases. Since the formulated problems are generally non-convex, it is not trivial to solve them optimally. Also, because of the dynamic mode switching process of the antennas, conventional approaches for the UTS methods cannot be directly extended to our scenario.

First, for the linear EH model, the globally optimal solution for the rate maximization problem is presented. We first determine the optimal transmit covariance matrices by using the Lagrange duality, and then with the optimal precoding matrices, we obtain the optimal time durations via the subgradient method. Next, for the non-linear EH model, we apply the successive convex approximation (SCA) framework [25] which successively solves approximated convex problems of the original non-convex one. By deriving new convex surrogate functions for the non-convex non-linear EH constraints, an efficient algorithm is provided for the rate maximization problem which yields a local optimal solution. Moreover, we propose a low-complexity algorithm of the DTS protocol by properly selecting the mode of each receive antenna, which achieves near-optimal performance with much reduced complexity. Numerical results confirm that the proposed TS architectures offer a significant performance gain over the conventional UTS.

This paper is organized as follows: In Section II, we introduce a system model and formulate the rate maximization problems for the DTS protocol. The globally optimal algorithm for the linear EH model is provided in Section III, and Section IV presents an efficient algorithm for the non-linear EH model. In Section V, we evaluate the R-E performance of the proposed algorithms through numerical simulations. Finally, the paper is terminated with conclusions in Section VI.

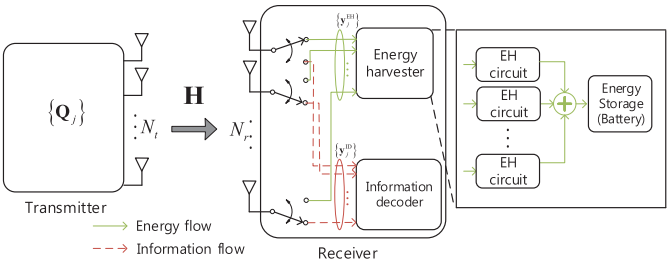

Fig. 1. Schematic diagram for MIMO SWIPT systems.

Throughout this paper, we employ uppercase boldface letters, lowercase boldface letters, and normal letters for matrices, vectors, and scalar quantities, respectively. A set of all complex matrices of size m-by-n is represented by $\mathbb{C}^{m\times n}$. Also, diag$(x_1,\cdots,x_m)$ stands for a diagonal matrix with diagonal elements $x_1,\cdots,x_m$, and $\mathbf{I}_m$ indicates an identity matrix of size m-by-m. For a matrix $\mathbf{M}$, tr$(\mathbf{M})$ and rank$(\mathbf{M})$ denote trace and rank of $\mathbf{M}$, respectively. The operation $(\cdot)^H$ represents conjugate transpose, $\mathbb{E}[\cdot]$ means statistical expectation, and $||\mathbf{x}||$ is the Euclidean norm of a complex vector $\mathbf{x}$. Also, $|x|$ indicates the magnitude of a complex scalar x, $(x)^+$ is defined as $\max\{0,x\}$, and $\frac{\partial f(x)}{\partial x}$ accounts for the partial derivative of a function $f(x)$ with respect to a variable x. When applied to a set $\mathcal{X}$, $|\mathcal{X}|$ and $\mathcal{X}^c$ stand for the cardinality and the complement of $\mathcal{X}$, respectively.

II. System Model

As illustrated in Fig. 1, we consider a P2P MIMO SWIPT system where a transmitter with N_t antennas sends information and energy signals to a receiver equipped with N_r antennas. We adopt the TS-based SWIPT protocol [4] which switches the operation of the receiver between the ID and the EH modes. Unlike the conventional UTS protocol where a single TS circuit is employed for all receive antennas [4], in this paper, we investigate a general DTS scenario where each receive antenna utilizes its own TS circuit. Therefore, the receiver can individually change the roles of each antenna to improve the SWIPT performance.

In the DTS, according to the operations of the receive antennas, there exist total 2^{N_r} different antenna modes. To identify the optimal performance of the TS-based SWIPT, we illustrate the DTS frame structure in Fig. 2 that consists of 2^{N_r} phases, each of which corresponds to each antenna mode.[1] We denote δ_j as the time duration of phase j $(j=1,\cdots,2^{N_r})$, and the total transmission time for one system block is set to one as

$$\sum_{j=1}^{2^{N_r}} \delta_j = 1. \tag{1}$$

[1]For a low-complexity implementation, one could select $D \le N_r+1$ antenna modes out of total 2^{N_r} possible candidates. This will be presented in Sec. III-C.

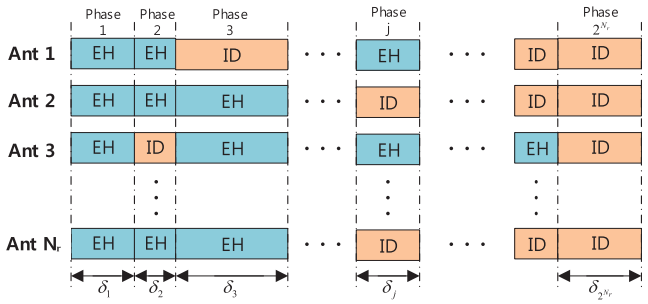

Fig. 2. Frame structure of the proposed DTS protocol.

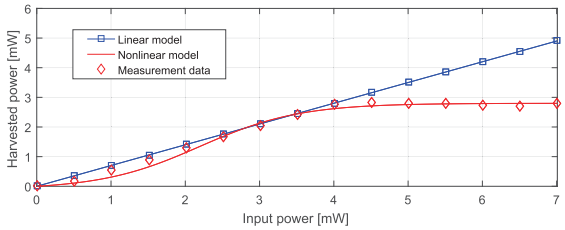

Fig. 3. A comparison between the EH models with $\eta = 0.7$, $M = 2.8$ mW, $a = 1500$, and $b = 0.0022$.

To characterize the antenna mode at each phase, let us define $\mathcal{I}_j \triangleq \{i_{1,j}, i_{2,j}, \cdots, i_{M_j,j}\} \subset \mathcal{N}_r \triangleq \{1, \cdots, N_r\}$ and $\mathcal{E}_j \triangleq \{e_{1,j}, e_{2,j}, \cdots, e_{W_j,j}\} = \mathcal{N}_r - \mathcal{I}_j$ as the sets of the antenna indices operating in the ID and the EH modes in phase j, respectively, where M_j is the cardinality of $\mathcal{I}_j$ and $W_j = N_r - M_j$ stands for that of $\mathcal{E}_j$. Then, the received signals at antennas $\mathcal{I}_j$ are utilized for the ID, while those at the remaining antennas $\mathcal{E}_j$ are passed to the EH circuit. It is assumed that all the antennas in the first and the last phase act as the EH and the ID modes, respectively, i.e., $\mathcal{E}_1 = \mathcal{N}_r$, $\mathcal{I}_1 = \emptyset$, $\mathcal{E}_{2^{N_r}} = \emptyset$, and $\mathcal{I}_{2^{N_r}} = \mathcal{N}_r$. Hence, the conventional UTS can be regarded as a special case of the proposed DTS by setting $\delta_2 = \cdots = \delta_{2^{N_r}-1} = 0$.

Let us denote $\mathbf{H} = [\mathbf{h}_1, \cdots, \mathbf{h}_{N_r}]^H \in \mathbb{C}^{N_r \times N_t}$ as the channel matrix from the transmitter to the receiver which is constant over one system block, where $\mathbf{h}_k \in \mathbb{C}^{N_t \times 1}$ for $k = 1, \cdots, N_r$ indicates the channel vector between the transmitter and the k-th receive antenna. In phase j, the receiver collects the signals $\mathbf{y}_j^{\text{ID}} \in \mathbb{C}^{M_j \times 1}$ and $\mathbf{y}_j^{\text{EH}} \in \mathbb{C}^{W_j \times 1}$ for the ID and the EH, respectively, which can be written by

$$\begin{aligned} \mathbf{y}_j^{\text{ID}} &= \mathbf{H}_j \mathbf{x}_j + \mathbf{n}_j^{\text{ID}}, \\ \mathbf{y}_j^{\text{EH}} &= \mathbf{G}_j \mathbf{x}_j + \mathbf{n}_j^{\text{EH}}, \end{aligned} \tag{2}$$

where $\mathbf{H}_j \triangleq [\mathbf{h}_{i_{1,j}} \cdots \mathbf{h}_{i_{M_j,j}}]^H \in \mathbb{C}^{M_j \times N_t}$ and $\mathbf{G}_j \triangleq [\mathbf{h}_{e_{1,j}} \cdots \mathbf{h}_{e_{W_j,j}}]^H \in \mathbb{C}^{W_j \times N_t}$ respectively stand for the channel matrices for the ID and the EH antennas, $\mathbf{x}_j \in \mathbb{C}^{N_t \times 1}$ indicates the transmitted signal in phase j with covariance matrix $\mathbb{E}[\mathbf{x}_j \mathbf{x}_j^H] = \mathbf{Q}_j \in \mathbb{C}^{N_t \times N_t}$, and $\mathbf{n}_j^{\text{ID}} \in \mathbb{C}^{M_j \times 1}$ and $\mathbf{n}_j^{\text{EH}} \in \mathbb{C}^{W_j \times 1}$ represent the zero-mean complex Gaussian noise vectors of the ID and the EH antennas with covariance matrices $\mathbf{I}_{M_j}$ and $\mathbf{I}_{W_j}$, respectively. We assume that perfect CSI is available both at the transmitter and the receiver, which can be achieved by estimating the overall MIMO channel matrix $\mathbf{H}$ with the aid of standard channel estimation processes [4], [7]. Notice that we focus on the indoor environment scenario where the channel matrix $\mathbf{H}$ is assumed to be fixed during one system block.

The transmit covariance matrices $\{\mathbf{Q}_j\}$ are subject to the following power constraints

$$\sum_{j=1}^{2^{N_r}} \delta_j \text{tr}(\mathbf{Q}_j) \le P_A, \tag{3}$$

$$\text{tr}(\mathbf{Q}_j) \le P_P, \quad \text{for } j = 1, \cdots, 2^{N_r}, \tag{4}$$

where (3) accounts for the average power in Watt·sec and (4) indicates the peak power budget in Watt at the transmitter. From (2), the achievable rate R_j in phase j is expressed as

$$R_j = \delta_j \log \left| \mathbf{I}_{M_j} + \mathbf{H}_j \mathbf{Q}_j \mathbf{H}_j^H \right|.$$

As a result, the total data rate R_{tot} of the DTS protocol over one system block is given by $R_{tot} = \sum_{j=2}^{2^{N_r}} R_j$.

Now, we explain the EH process of the proposed DTS protocol. Let us define a function $\Delta(x)$ which reflects the EH process of rectifier circuits for a given input power x. Then, by utilizing multiple EH circuits with a DC combiner [26], the total harvested energy E in Watt·sec can be computed as

$$\begin{aligned} E &= \sum_{j=1}^{2^{N_r}-1} \sum_{i=1}^{W_j} \delta_j \Delta\left(\mathbb{E}\left[\left| y_{i,j}^{\text{EH}} \right|^2 \right] \right) \\ &\approx \sum_{j=1}^{2^{N_r}-1} \sum_{i=1}^{W_j} \delta_j \Delta\left(\mathbf{h}_{e_{i,j}}^H \mathbf{Q}_j \mathbf{h}_{e_{i,j}} \right), \end{aligned} \tag{5}$$

where $y_{i,j}^{\text{EH}}$ represents the signal received at antenna i in phase j, and the noise power is ignored in (5) since it is practically much smaller than the transmitted signal power [4], [24]. Due to the non-linearity of practical rectifiers, it is not easy to derive analytical expressions for $\Delta(x)$.

To address this issue, there have been several studies to obtain accurate approximations of $\Delta(x)$ [4], [20], [22]. Since the EH process function $\Delta(x)$ is monotonically increasing with input power x, in the linear EH model [4], $\Delta(x)$ is approximated as $\Delta(x) \simeq \Delta_{\text{L}}(x) \triangleq \eta x$ where $\eta \in (0, 1]$ indicates the EH efficiency. The linear EH model allows simple and low-complexity approaches for the transceiver designs thanks to the analytically tractable form [12]–[17].

Also, the non-linear EH model $\Delta_{\text{NL}}(x)$ in [22] is expressed as

$$\Delta_{\text{NL}}(x) = \frac{M}{1-c} \left(\frac{1}{1 + \exp\left(-ax + ab\right)} - c \right), \tag{6}$$

where $c \triangleq \frac{1}{1+\exp(ab)}$, the constant M characterizes the maximum harvested power at which the EH circuit is saturated, and a and b are related to the EH circuit specifications such as capacitance and diode turn-on voltage. In practice, the parameters M, a and b can be identified by a standard curve fitting tool based on measurement data [20]. Fig. 3 compares the linear and non-linear EH models with the measurement data of the harvested power. It is illustrated that both the EH models are well-matched with the experimental results when

the received signal power is small, while the limitation of the linear model is revealed as the power goes high.

In this paper, we consider both the linear and non-linear EH models $\Delta_{\mathrm{L}}(x)$ and $\Delta_{\mathrm{NL}}(x)$. To fully analyze the SWIPT performance of the proposed DTS protocol, we aim to identify the boundary points of the achievable R-E region $\mathcal{C}_{\mathrm{X}}^{\text{R-E}}$ for each EH model $\mathrm{X} \in \{\mathrm{L}, \mathrm{NL}\}$ under the average power and the peak power constraints in (3) and (4), respectively, as well as the total time constraint in (1). The achievable R-E region $\mathcal{C}_{\mathrm{X}}^{\text{R-E}}$ is defined as

$$\mathcal{C}_{\mathrm{X}}^{\text{R-E}} \triangleq \Bigg\{(R,E): R \leq \sum_{j=2}^{2^{N_r}} \delta_j \log\left|\mathbf{I}_{M_j} + \mathbf{H}_j\mathbf{Q}_j\mathbf{H}_j^H\right|, \\ E \leq \sum_{j=1}^{2^{N_r}-1}\sum_{i=1}^{W_j} \delta_j \Delta_{\mathrm{X}}\left(\mathbf{h}_{e_{i,j}}^H \mathbf{Q}_j \mathbf{h}_{e_{i,j}}\right), \\ \mathrm{tr}(\mathbf{Q}_j) \leq P_P, \quad \forall j, \ \sum_{j=1}^{2^{N_r}} \delta_j \mathrm{tr}(\mathbf{Q}_j) \leq P_A, \ \sum_{j=1}^{2^{N_r}} \delta_j = 1\Bigg\}.$$

Then, the boundary points of $\mathcal{C}_{\mathrm{X}}^{\text{R-E}}$ can be found by solving the following rate maximization problem

$$\text{(P)} \quad \max_{\{\mathbf{Q}_j \succeq 0\}, \{\delta_j \geq 0\}} \ \sum_{j=2}^{2^{N_r}} \delta_j \log\left|\mathbf{I}_{M_j} + \mathbf{H}_j\mathbf{Q}_j\mathbf{H}_j^H\right| \\ \text{s.t.} \ \sum_{j=1}^{2^{N_r}-1}\sum_{i=1}^{W_j} \delta_j \Delta_{\mathrm{X}}\left(\mathbf{h}_{e_{i,j}}^H \mathbf{Q}_j \mathbf{h}_{e_{i,j}}\right) \geq \bar{E}, \tag{7} \\ \mathrm{tr}(\mathbf{Q}_j) \leq P_P, \quad \forall j, \ \sum_{j=1}^{2^{N_r}} \delta_j \mathrm{tr}(\mathbf{Q}_j) \leq P_A, \sum_{j=1}^{2^{N_r}} \delta_j = 1,$$

where $\bar{E}$ denotes the minimum required harvested energy constraint. Due to the non-convex objective function and the constraint in (7), the rate maximization problem (P) is non-convex in general. Note that problem (P) can be regarded as a generalization of the conventional UTS design in [4] by including multiple modes. To be specific, unlink the system in [4] which only considered two phases, we need to jointly optimize the covariance matrices and the time durations for multiple phases. Therefore, the analysis and the approaches in [4], e.g., a closed-form time duration solution for two phases, are no longer valid in our DTS protocol in (P). Also, the linear EH model solution in [4] cannot be directly applied to (P) with the practical non-linear EH circuit case. Thus, it is not straightforward to determine the globally optimal solution for (P) with existing algorithms.

By solving (P) for all feasible EH constraint $0 \leq \bar{E} \leq \bar{E}_{max}$, where $\bar{E}_{max}$ stands for the maximum harvested energy, we can determine the achievable R-E region of the DTS protocol. It is easy to show that the maximum harvested energy $\bar{E}_{max}$ in the DTS can be achieved by setting $\delta_1 = 1$ and $\delta_j = 0$ for $j = 2, \cdots, 2^{N_r}$, i.e., all the received signals are utilized for the EH during one system block. Thus, denoting $\lambda_{\mathbf{G}_j,l}$ and $\mathbf{v}_{\mathbf{G}_j,l}$ as the l-th largest eigenvalue of $\mathbf{G}_j^H\mathbf{G}_j$ and its corresponding eigenvector, respectively, $\bar{E}_{max}$ can be attained with the optimal transmit covariance matrix $\mathbf{Q}_1^\star = P_A \mathbf{v}_{\mathbf{G}_1,1}\mathbf{v}_{\mathbf{G}_1,1}^H$ as[2] [4], [24]

$$\bar{E}_{max} = \Delta_{\mathrm{X}}(P_A \lambda_{\mathbf{G}_1,1}).$$

III. Optimal Solution for the Linear EH Model

In this section, we present the globally optimal solution of (P) for the linear EH model. To tackle the non-convexity, let us introduce a change of variables as $\hat{\mathbf{Q}}_j \triangleq \delta_j \mathbf{Q}_j$ for $j = 1, \cdots, 2^{N_r}$. Then, (P) for the linear EH model is reformulated as

$$\text{(P1)} \quad \max_{\{\hat{\mathbf{Q}}_j \succeq 0\}, \{\delta_j \geq 0\}} \ \sum_{j=2}^{2^{N_r}} \delta_j \log\left|\mathbf{I}_{M_j} + \frac{1}{\delta_j}\mathbf{H}_j\hat{\mathbf{Q}}_j\mathbf{H}_j^H\right| \\ \text{s.t.} \ \eta \sum_{j=1}^{2^{N_r}-1} \mathrm{tr}\left(\mathbf{G}_j\hat{\mathbf{Q}}_j\mathbf{G}_j^H\right) \geq \bar{E}, \tag{8} \\ \sum_{j=1}^{2^{N_r}} \mathrm{tr}(\hat{\mathbf{Q}}_j) \leq P_A, \tag{9} \\ \mathrm{tr}(\hat{\mathbf{Q}}_j) \leq \delta_j P_P, \quad \text{for } j = 1, \cdots, 2^{N_r}, \tag{10} \\ \sum_{j=1}^{2^{N_r}} \delta_j = 1. \tag{11}$$

One can see that the objective function of (P1) is the perspective of the log-determinant which is a concave function. Since the perspective operation preserves the concavity [27], we can conclude that the objective function is jointly concave with respect to $\{\hat{\mathbf{Q}}_j\}$ and $\{\delta_j\}$. In the following, we first derive analytic expressions of the optimal transmit covariance matrices $\{\hat{\mathbf{Q}}_j^\star\}$ with fixed time $\{\delta_j\}$, and then address a method for determining the optimal durations $\{\delta_j^\star\}$. Our approach ensures optimality since (P1) is jointly convex with respect to $\{\hat{\mathbf{Q}}_j\}$ and $\{\delta_j\}$.[3]

A. Optimal Transmit Covariance Matrices

In this subsection, we introduce the analytical results of $\{\hat{\mathbf{Q}}_j^\star\}$ of problem (P1) for given $\{\delta_j\}$. As (P1) is convex and satisfies the Slaster's condition [27], it has zero duality gap. Therefore, the problem can be optimally solved by using the Lagrange duality method. The Lagrangian of (P1) is formulated as

$$\mathcal{L}\left(\{\hat{\mathbf{Q}}_j\}, \mu, \beta, \{\nu_j\}\right) \\ = \sum_{j=2}^{2^{N_r}} \delta_j \log\left|\mathbf{I}_{M_j} + \frac{1}{\delta_j}\mathbf{H}_j\hat{\mathbf{Q}}_j\mathbf{H}_j^H\right| - \mu\bar{E} + \beta P_A \\ - \sum_{j=1}^{2^{N_r}} \mathrm{tr}\left(\mathbf{A}_j(\mu, \beta, \{\nu_j\})\hat{\mathbf{Q}}_j\right) + P_P \sum_{j=1}^{2^{N_r}} \nu_j\delta_j, \tag{12}$$

[2]The maximum information rate can be achieved by setting $\delta_{2^{N_r}} = 1$. Here, the optimal covariance matrix $\mathbf{Q}_{2^{N_r}}$ is given by the water-filling solution [4, eq. (3)].

[3]Thanks to the joint convexity of (P1), one might first obtain $\{\delta_j^\star\}$, and then compute $\{\hat{\mathbf{Q}}_j^\star\}$ without loss of optimality.

where μ, β, and $\{\nu_j\}$ are the non-negative Lagrangian multipliers associated with the constraint in (8), (9), and (10), respectively, and $\mathbf{A}_j(\mu,\beta,\{\nu_j\}) \triangleq (\beta+\nu_j)\mathbf{I}_{N_t} - \mu\eta\mathbf{G}_j^H\mathbf{G}_j$. Here, we define $\mathbf{G}_{2^{N_r}} \triangleq \mathbf{0}$ for notational convenience.

Then, the dual function $\mathcal{G}(\mu,\beta,\{\nu_j\})$ of (P1) can be expressed as $\mathcal{G}(\mu,\beta,\{\nu_j\}) = \max_{\{\hat{\mathbf{Q}}_j\succeq 0\}} \mathcal{L}\left(\{\hat{\mathbf{Q}}_j\},\mu,\beta,\{\nu_j\}\right)$, and the corresponding dual problem is given by

$$\min_{\mu\geq 0,\beta\geq 0,\{\nu_j\geq 0\}} \mathcal{G}(\mu,\beta,\{\nu_j\}). \tag{13}$$

Thus, to obtain $\{\hat{\mathbf{Q}}_j^\star\}$, we first calculate the dual function $\mathcal{G}(\mu,\beta,\{\nu_j\})$, and then determine the optimal dual variables $\mu^\star,\beta^\star$, and $\{\nu_j^\star\}$ by solving (13).

Denoting $\mathcal{S}$ as the set of phase indices j such that $j\neq 1$ and $\delta_j>0$, the Lagrangian (12) can be rewritten by

$$\mathcal{L}\left(\{\hat{\mathbf{Q}}_j\},\mu,\beta,\{\nu_j\}\right) = \sum_{j=1}^{2^{N_r}} \mathcal{L}_j\left(\hat{\mathbf{Q}}_j,\mu,\beta,\nu_j\right) - \mu\bar{E} + \beta P_A + P_P\sum_{j=1}^{2^{N_r}}\nu_j\delta_j,$$

where

$$\mathcal{L}_j\left(\hat{\mathbf{Q}}_j,\mu,\beta,\nu_j\right) \triangleq \begin{cases} \delta_j \log\left|\mathbf{I}_{M_j} + \frac{1}{\delta_j}\mathbf{H}_j\hat{\mathbf{Q}}_j\mathbf{H}_j^H\right| - \mathrm{tr}\big(\mathbf{A}_j(\mu,\beta,\{\nu_j\})\hat{\mathbf{Q}}_j\big), \\ \quad \text{for } j\in\mathcal{S}, \\ -\mathrm{tr}\big(\mathbf{A}_j(\mu,\beta,\{\nu_j\})\hat{\mathbf{Q}}_j\big), \quad \text{for } j\in\mathcal{S}^c. \end{cases}$$

Since the function $\mathcal{L}_j\left(\hat{\mathbf{Q}}_j,\mu,\beta,\nu_j\right)$ depends only on $\hat{\mathbf{Q}}_j$ with given $\{\delta_j\}$, we can identify the dual function by solving the following 2^{N_r} individual problems

$$\max_{\hat{\mathbf{Q}}_j\succeq 0} \ \mathcal{L}_j\left(\hat{\mathbf{Q}}_j,\mu,\beta,\nu_j\right), \quad \text{for } j=1,\cdots,2^{N_r}. \tag{14}$$

We first consider (14) for $j\in\mathcal{S}$. In this case, $\mathbf{A}_j(\mu^\star,\beta^\star,\{\nu_j^\star\})$ must be a positive definite matrix, since otherwise a solution for (14) becomes infeasible as $\hat{\mathbf{Q}}_j^\star = \alpha\mathbf{z}_j\mathbf{z}_j^H$ with $\alpha\to\infty$, where $\mathbf{z}_j$ stands for the eigenvector of $\mathbf{A}_j(\mu^\star,\beta^\star,\{\nu_j^\star\})$ associated with any non-positive eigenvalues. As a result, the optimal dual variables $\mu^\star$, $\beta^\star$, and $\{\nu_j^\star\}$ should satisfy

$$\beta^\star + \nu_j^\star > \mu^\star\eta\lambda_{\mathbf{G}_j,1}, \quad \text{for } j\in\mathcal{S}. \tag{15}$$

Based on (15), we can determine the optimal solution $\hat{\mathbf{Q}}_j^\star$ to (14) for $j\in\mathcal{S}$ as [4]

$$\hat{\mathbf{Q}}_j^\star = \delta_j\mathbf{A}_j^{-\frac{1}{2}}\tilde{\mathbf{V}}_j\mathbf{\Sigma}_j\tilde{\mathbf{V}}_j^H\mathbf{A}_j^{-\frac{1}{2}}, \quad \text{for } j\in\mathcal{S}, \tag{16}$$

where $\tilde{\mathbf{V}}_j$ represents the right singular vector matrix of $\mathbf{H}_j\mathbf{A}_j^{-\frac{1}{2}}$ and the diagonal matrix $\mathbf{\Sigma}_j$ is defined as $\mathbf{\Sigma}_j = \mathrm{diag}\left(\tilde{p}_{j,1},\cdots,\tilde{p}_{j,M}\right)$ with $\tilde{p}_{j,m} = \left(1/\log 2 - 1/\tilde{h}_{j,m}\right)^+$. Here, $\tilde{h}_{j,m}$ for $m=1,\cdots,M$ indicates the singular value of $\mathbf{H}_j\mathbf{A}_j^{-\frac{1}{2}}$ where M equals $M=\min(N_t,N_r)$.

Next, for $j\in\mathcal{S}^c$, the problem in (14) becomes convex semi-definite programming (SDP), whose necessary and sufficient optimality conditions can be written as [28]

$$\mathbf{A}_j(\mu^\star,\beta^\star,\{\nu_j^\star\})\hat{\mathbf{Q}}_j^\star = \mathbf{0}, \tag{17}$$

$$\hat{\mathbf{Q}}_j^\star \succeq \mathbf{0}, \tag{18}$$

$$\mathbf{A}_j(\mu^\star,\beta^\star,\{\nu_j^\star\}) \succeq \mathbf{0}, \tag{19}$$

where (17) and (18) stand for the Karush-Kuhn-Tucker (KKT) conditions and (19) is obtained since otherwise the dual function goes to infinity. Then, for two individual cases in which all eigenvalues of $\mathbf{A}_j(\mu^\star,\beta^\star,\{\nu_j^\star\})$ are either positive or not, we can determine $\hat{\mathbf{Q}}_j^\star$ for $j\in\mathcal{S}^c$ from (17)-(19) as

$$\hat{\mathbf{Q}}_j^\star = \begin{cases} \mathbf{0}, & \text{for } \beta^\star+\nu_j^\star > \mu^\star\eta\lambda_{\mathbf{G}_j,1}, \\ \alpha_j\mathbf{v}_{\mathbf{G}_j,1}\mathbf{v}_{\mathbf{G}_j,1}^H, & \text{for } \beta^\star+\nu_j^\star = \mu^\star\eta\lambda_{\mathbf{G}_j,1}, \end{cases} \tag{20}$$

where α_j is any non-negative number. One can easily check that the solution in (20) fulfills the optimality conditions in (17) and (18).

By substituting the optimal $\{\hat{\mathbf{Q}}_j^\star\}$ into (12), the dual problem in (13) can be given by

$$\begin{aligned} \min_{\mu\geq 0,\beta\geq 0,\{\nu_j\geq 0\}} \ & \mathcal{L}\left(\{\hat{\mathbf{Q}}_j^\star\},\mu,\beta,\{\nu_j\}\right) \\ \text{s.t. } & \beta^\star+\nu_j^\star > \mu^\star\eta\lambda_{\mathbf{G}_j,1}, \quad \text{for } j\in\mathcal{S}, \\ & \beta^\star+\nu_j^\star \geq \mu^\star\eta\lambda_{\mathbf{G}_j,1}, \quad \text{for } j\in\mathcal{S}^c. \end{aligned}$$

Due to the convexity of the dual problem, it can be optimally solved by employing the sub-gradient method, e.g., the ellipsoid method [27]. The sub-gradient g_μ, g_β, and $\{g_{\nu_j}\}$ of the dual function with respect to μ, β, and $\{\nu_j\}$ are respectively expressed as

$$g_\mu = \eta\sum_{j=1}^{2^{N_r}-1}\mathrm{tr}\left(\mathbf{G}_j\hat{\mathbf{Q}}_j^\star\mathbf{G}_j^H\right) - \bar{E}, \tag{21}$$

$$g_\beta = P_A - \sum_{j=1}^{2^{N_r}}\mathrm{tr}(\hat{\mathbf{Q}}_j^\star), \tag{22}$$

$$g_{\nu_j} = P_P\delta_j - \mathrm{tr}(\hat{\mathbf{Q}}_j^\star), \quad \text{for } j=1,\cdots,2^{N_r}. \tag{23}$$

B. Optimal Time Durations

So far, we have derived the optimal transmit covariance matrices $\{\hat{\mathbf{Q}}_j^\star\}$ for given $\{\delta_j\}$. In this subsection, we present the optimal time durations $\{\delta_j^\star\}$ for (P1). To this end, let us first define $\{\tilde{\mathbf{Q}}_j\}$ as the transmit covariance matrices which maximize the harvested energy with fixed $\{\delta_j\}$. Then, we consider the harvested energy maximization problem with given $\{\delta_j\}$ as

$$\tilde{E}(\{\delta_j\}) \triangleq \max_{\{\tilde{\mathbf{Q}}_j\succeq 0\}} \sum_{j=1}^{2^{N_r}-1}\mathrm{tr}\left(\mathbf{G}_j\tilde{\mathbf{Q}}_j\mathbf{G}_j^H\right) \tag{24}$$

$$\text{s.t. } \sum_{j=1}^{2^{N_r}}\mathrm{tr}(\tilde{\mathbf{Q}}_j) \leq P_A, \tag{25}$$

$$\mathrm{tr}(\tilde{\mathbf{Q}}_j) \leq P_P\delta_j, \quad \text{for } j=1,\cdots,2^{N_r}, \tag{26}$$

where $\tilde{E}(\{\delta_j\})$ represents the optimal value of problem (24), which reflects the maximum achievable harvested energy with given $\{\delta_j\}$. Notice that the problem in (24) reveals the feasibility of (P1) for fixed $\{\delta_j\}$. To be specific, (P1) is feasible when $\tilde{E}(\{\delta_j\}) \geq \bar{E}$, while it becomes infeasible for $\tilde{E}(\{\delta_j\}) < \bar{E}$. Therefore, the optimal $\{\delta_j^\star\}$ must be found under the feasibility condition $\tilde{E}(\{\delta_j\}) \geq \bar{E}$. In the following lemma, we provide the optimal value of $\tilde{E}(\{\delta_j\})$.

Lemma 1: Without loss of generality, suppose that phases are sorted such that $\lambda_{\mathbf{G}_j,1} > \lambda_{\mathbf{G}_k,1}$ for $j < k$. Then, the maximum harvest energy $\tilde{E}(\{\delta_j\})$ with fixed $\{\delta_j\}$ in the DTS can be calculated as

$$\tilde{E}(\{\delta_j\}) = P_P \sum_{j=1}^{N-1} \lambda_{\mathbf{G}_j,1}\delta_j + \left(P_A - P_P \sum_{j=1}^{N-1} \delta_j\right) \lambda_{\mathbf{G}_N,1},$$

where $\lambda_{\mathbf{G}_{2^{N_r}},1} \triangleq 0$ and N is defined as a minimum integer $n \in [1, 2^{N_r}]$ that satisfies $\sum_{j=1}^{n} \delta_j > \frac{P_A}{P_P}$.

Proof: See Appendix A. ∎

From Lemma 1, we obtain an analytic expression for $\tilde{E}(\{\delta_j\})$, which is an affine function with respect to $\{\delta_j\}$ when N is fixed. However, since the intermediate term N is a function of $\{\delta_j\}$, it is not easy to directly check the concavity of $\tilde{E}(\{\delta_j\})$. Nonetheless, in the following lemma, we elaborate on the concavity of $\tilde{E}(\{\delta_j\})$ through a rigorous verification.

Lemma 2: $\tilde{E}(\{\delta_j\})$ is a concave function over $\{\delta_j\}$.

Proof: See Appendix B. ∎

We denote $\mathcal{B}(\{\delta_j\}) \triangleq \sum_{j=2}^{2^{N_r}} \delta_j \log\left|\mathbf{I}_{M_j} + \frac{1}{\delta_j}\mathbf{H}_j\hat{\mathbf{Q}}_j^\star\mathbf{H}_j^H\right|$ as the optimal value of (P1) for given $\{\delta_j\}$. Then, from Lemma 1, the problem for computing $\{\delta_j^\star\}$ can be formulated as

$$\max_{\{\delta_j \geq 0\}} \ \mathcal{B}(\{\delta_j\}) \tag{27}$$

$$\text{s.t. } \tilde{E}(\{\delta_j\}) \geq \bar{E}, \tag{28}$$

$$\sum_{j=1}^{2^{N_r}} \delta_j = 1.$$

Since the strong duality holds for the original (P1), we can rewrite $\mathcal{B}(\{\delta_j\})$ as

$$\begin{aligned}\mathcal{B}(\{\delta_j\}) &= \min_{\mu,\beta\geq 0,\{\nu_j\geq 0\}} \mathcal{G}(\mu,\beta,\{\nu_j\}) \\ &= \sum_{j=1}^{2^{N_r}} \mathcal{L}_j\left(\hat{\mathbf{Q}}_j^\star, \mu^\star, \beta^\star, \nu_j^\star\right) - \mu^\star\bar{E} + \beta^\star P_A \\ &\quad + P_P \sum_{j=1}^{2^{N_r}} \nu_j^\star\delta_j. \end{aligned} \tag{29}$$

Also, by substituting $\delta_1 = 1 - \sum_{j=2}^{2^{N_r}} \delta_j$ into (28) and (29), it follows

$$\begin{aligned}\tilde{E}(\{\delta_j\}) &= P_P(\lambda_{\mathbf{G}_N,1} - \lambda_{\mathbf{G}_1,1}) \sum_{j=2}^{2^{N_r}} \delta_j + P_P(\lambda_{\mathbf{G}_1,1} - \lambda_{\mathbf{G}_N,1}) \\ &\quad + P_P \sum_{j=2}^{N-1} (\lambda_{\mathbf{G}_j,1} - \lambda_{\mathbf{G}_N,1})\delta_j + P_A\lambda_{\mathbf{G}_N,1} \\ &\geq \bar{E}, \end{aligned} \tag{30}$$

Algorithm 1 Optimal Algorithm for Solving (P1)

Initialize $\{\hat{\mathbf{Q}}_j \succeq 0\}$, $\{\delta_j \geq 0\}$, $\mu \geq 0$, $\beta \geq 0$, and $\nu_j \geq 0$ for $j = 1, \cdots, 2^{N_r}$.
Repeat
  Repeat
    Compute $\left\{\hat{\mathbf{Q}}_j^\star\right\}$ using (16) and (20) with given μ, β, and $\{\nu_j\}$.
    Compute the subgradient of $\mathcal{G}(\mu,\beta,\{\nu_j\})$ using (21), (22), and (23).
    Update μ, β, and $\{\nu_j\}$ using the ellipsoid method [30].
  Until μ, β, and $\{\nu_j\}$ converge to the prescribed accuracy.
  Compute the subgradient of $\mathcal{F}(\{\delta_j\})$ using (33).
  Update δ_j for $j = 2, \cdots, 2^{N_r}$ using the ellipsoid method.
Until $\{\delta_j\}$ converge to the prescribed accuracy.

$$\begin{aligned}\mathcal{B}(\{\delta_j\}) &= \mathcal{F}(\{\delta_j\}) - \mu^\star\bar{E} + \beta^\star P_A + P_P\nu_1^\star \\ &\quad - \sum_{j=1}^{2^{N_r}} \mathrm{tr}\left(\left\{(\beta^\star + \nu_j^\star)\mathbf{I}_{N_t} - \mu^\star\eta\mathbf{G}_j^H\mathbf{G}_j\right\}\hat{\mathbf{Q}}_j^\star\right), \end{aligned} \tag{31}$$

where

$$\mathcal{F}(\{\delta_j\}) \triangleq \sum_{j=2}^{2^{N_r}} \delta_j \left(\log\left|\mathbf{I}_{M_j} + \frac{1}{\delta_j}\mathbf{H}_j\hat{\mathbf{Q}}_j^\star\mathbf{H}_j^H\right| + P_P(\nu_j^\star - \nu_1^\star)\right).$$

As a result, from (30) and (31), the problem in (27) can be recast to

$$\max_{\{\delta_j \geq 0\}} \ \mathcal{F}(\{\delta_j\}) \tag{32}$$

$$\text{s.t. } \sum_{j=2}^{2^{N_r}} \delta_j \leq 1 \ \text{ and (30)}.$$

Owing to the convexity of (32), we can optimally solve it via the sub-gradient method. The sub-gradient g_{δ_j} of $\mathcal{F}(\{\delta_j\})$ with respect to δ_j for $j = 2, \cdots, 2^{N_r}$ is given by

$$\begin{aligned}g_{\delta_j} &= \log\left|\mathbf{I}_{M_j} + \frac{1}{\delta_j}\mathbf{H}_j\hat{\mathbf{Q}}_j^\star\mathbf{H}_j^H\right| + P_p(\nu_j^\star - \nu_1^\star) - M_j \\ &\quad + \mathrm{tr}\left(\left(\mathbf{I}_{M_j} + \frac{1}{\delta_j}\mathbf{H}_j\hat{\mathbf{Q}}_j^\star\mathbf{H}_j^H\right)^{-1}\right), \end{aligned} \tag{33}$$

which comes from the fact $\partial\det(\mathbf{M}) = \det(\mathbf{M})\mathrm{tr}\left(\mathbf{M}^{-1}\partial\mathbf{M}\right)$ [29]. After obtaining the optimal $\delta_j^\star$ for $j = 2, \cdots, 2^{N_r}$, $\delta_1^\star$ can be easily computed by $\delta_1^\star = 1 - \sum_{j=2}^{2^{N_r}} \delta_j^\star$. To summarize, Algorithm 1 for solving (P1) is shown below, whose optimality and convergence have been proved in [27] and [30] for any given initial points. In our simulations, the dual variables μ, β, $\{\nu_j\}$ and the durations $\{\delta_j\}$ are initialized as $\mu = 10^4$, $\beta = 15$, $\nu_j = 10$, and $\delta_j = \frac{1}{2^{N_r}}$ for all j, respectively, and the prescribed accuracy which represents the stopping condition for the ellipsoid method is equal to 10^{-4}.

We briefly discuss the computational complexity of the proposed Algorithm 1. The optimal transmit precoding matrices $\{\hat{\mathbf{Q}}_j^\star\}$ are determined for given $\{\delta_j\}$ in an inner layer, and

then we calculate $\{\delta_j^\star\}$ in an outer layer. As the complexity of Algorithm 1 is dominated by two ellipsoid methods, each of which finds the dual variables and the optimal $\{\delta_j^\star\}$, respectively, the total complexity of Algorithm 1 becomes $\mathcal{O}(2^{4N_r})$ [27].

C. Low Complexity Algorithm With Antenna Mode Selection

In the preceding subsection, the optimal solution for the transmit covariance matrices and the time durations have been obtained when all possible 2^{N_r} antenna modes are included as in Fig. 2. Although this provides the optimal performance of the proposed DTS protocol, the computational complexity for the transceiver optimization process in Algorithm 1 is proportional to the number of antenna modes 2^{N_r}, which might be a burden for a large N_r.

To tackle this issue, we present a low-complexity algorithm of the proposed DTS with D phases.[4] In this approach, each receive antenna switches its operation only once from the EH mode to the ID mode. Accordingly, for each phase u ($u = 1, \cdots, D$), we have $\mathcal{I}_{u-1} \subset \mathcal{I}_u$. The low-complexity algorithm can reduce the implementation complexity since it only considers a small number of phases. Similar to the optimal frame structure in Fig. 2, we assume $\mathcal{I}_1 = \emptyset$ and $\mathcal{I}_D = \mathcal{N}_r$. Then, the performance would depend on the mode switching order of the receive antennas, since at phase u, the channel matrix $\mathbf{H}_u$ changes for each mode switching candidate. Hence, the search size becomes $\prod_{u=2}^{D-1}(N_r + 2 - u)$. To further reduce the complexity, we propose an antenna mode selection method for each phase u as follows.

Let $\mathcal{T}_u \triangleq \left\{\mathcal{I}_s \middle| M_s = u-1,\ \bar{\mathcal{I}}_{u-1} \subset \mathcal{I}_s \subset \mathcal{N}_r\right\}$ be the set of the antenna mode candidates for phase u, where $\bar{\mathcal{I}}_{u-1}$ is the antenna mode set, i.e., the set of antennas operating in the ID, selected for phase $(u-1)$. First, we initialize the iteration index u and the selected antenna mode set $\Omega(u)$ as $\Omega(u) = \left\{\bar{\mathcal{I}}_1 = \emptyset, \bar{\mathcal{I}}_D = \mathcal{N}_r\right\}$. Then, at iteration u, the antenna mode $\mathcal{I}_s \in \mathcal{T}_u$, which maximizes the total rate $\mathcal{R}\left(\Omega(u-1) \cup \{\mathcal{I}_s\}\right)$, is chosen for phase u, where we define $\mathcal{R}(\mathcal{X})$ as the total rate with the antenna mode set $\mathcal{X}$, which can be computed by optimizing the covariance matrices and durations with setting $\delta_j = 0$ for $\mathcal{I}_j \notin \mathcal{X}$ in Algorithm 1. The procedure is terminated when the rate does not increase any more or the cardinality of $\Omega(u)$ becomes $N_r + 1$. We summarize the proposed antenna mode selection method as below.

In Algorithm 2, since we only consider $N_r + 2 - u$ elements from $\mathcal{T}_u$ at iteration u for $u = 2, \cdots, D-1 \leq N_r$, the computational complexity can be expressed as $\mathcal{O}\big(\sum_{u=2}^{Nr}(u+1)^4(N_r + 2 - u)\big)$, which is much lower than that of the DTS scheme with the optimal frame structure. For example, for $N_r = 4$, the complexity order for the optimal DTS is 65,536, while that for the proposed low-complexity antenna mode selection becomes 2,342, which is only 3.56% of the optimal DTS. From the simulation, we will show that the proposed selection method achieves near-optimal performance.

[4]The design parameter D ($D \leq N_r + 1$) determines a tradeoff between the computational complexity and the SWIPT performance. Appropriate choices for D will be examined in Section V from numerical results.

Algorithm 2 Antenna Mode Selection Altorighm

Initialize $u \leftarrow 1$ and $\Omega(u) \leftarrow \left\{\bar{\mathcal{I}}_1 = \emptyset, \bar{\mathcal{I}}_D = \mathcal{N}_r\right\}$.
Repeat
  Set $u \leftarrow u + 1$.
  Set $\mathcal{T}_u = \left\{\mathcal{I}_s \middle| M_s = u-1,\ \bar{\mathcal{I}}_{u-1} \subset \mathcal{I}_s \subset \mathcal{N}_r\right\}$.
  Calculate $\mathcal{R}\left(\Omega(u-1) \cup \{\mathcal{I}_s\}\right)$ by optimizing $\{\hat{\mathbf{Q}}_j\}$ and $\{\delta_j\}$ via Algorithm 1.
  Calculate $\bar{\mathcal{I}}_u \leftarrow \arg\max_{\mathcal{I}_s \in \mathcal{T}_u} \mathcal{R}\left(\Omega(u-1) \cup \{\mathcal{I}_s\}\right)$.
  Set $\Omega(u) \leftarrow \Omega(u-1) \cup \left\{\bar{\mathcal{I}}_u\right\}$.
Until $\mathcal{R}(\Omega(u))$ does not increase **or** $|\Omega(u)| = N_r + 1$.

IV. Proposed Solution for the Non-Linear EH Model

In this section, we solve problem (P) for the non-linear EH model. With the EH constraint in (6), (P) can be equivalently formulated as

$$\text{(P2)} \quad \max_{\{\hat{\mathbf{Q}}_j \succeq 0\}, \{\delta_j \geq 0\}} \ \sum_{j=2}^{2^{N_r}} \delta_j \log \left| \mathbf{I}_{M_j} + \frac{1}{\delta_j} \mathbf{H}_j \hat{\mathbf{Q}}_j \mathbf{H}_j^H \right|$$

$$\text{s.t.} \ \sum_{j=1}^{2^{N_r}-1} \sum_{i=1}^{W_j} \delta_j \left(\frac{1}{1+\exp\left(-\frac{a}{\delta_j} \mathbf{h}_{e_{i,j}}^H \hat{\mathbf{Q}}_j \mathbf{h}_{e_{i,j}} + ab\right)} - c \right) \geq \frac{(1-c)\bar{E}}{M}, \tag{34}$$

$$(9),\ (10),\ \text{and}\ (11).$$

Due to the non-convexity of the sigmoidal function in the EH constraint (34), the proposed approach for the linear EH model in Sec. III cannot be directly applied to (P2).

To circumvent the problem, let us introduce slack variables $\tau_{i,j} \geq 0$ for $j = 1, \cdots, 2^{N_r} - 1$ and $i = 1, \cdots, W_j$, which represent the received RF signal power in phase j at the i-th antenna of the receiver. Denoting $\Xi(\delta_j, \tau_{i,j}) \triangleq \delta_j \Big/ \left(1 + \exp\left(-a\frac{\tau_{i,j}}{\delta_j} + ab\right)\right) - c\delta_j$, (P2) is transformed to

$$\text{(P2.1)} \quad \max_{\substack{\{\hat{\mathbf{Q}}_j \succeq 0\}, \{\delta_j \geq 0\} \\ \{\tau_{i,j} \geq 0\}}} \ \sum_{j=2}^{2^{N_r}} \delta_j \log \left| \mathbf{I}_{M_j} + \frac{1}{\delta_j} \mathbf{H}_j \hat{\mathbf{Q}}_j \mathbf{H}_j^H \right|$$

$$\text{s.t.} \ \sum_{j=1}^{2^{N_r}-1} \sum_{i=1}^{W_j} \Xi(\delta_j, \tau_{i,j}) \geq \frac{(1-c)\bar{E}}{M}, \tag{35}$$

$$\mathbf{h}_{e_{i,j}}^H \hat{\mathbf{Q}}_j \mathbf{h}_{e_{i,j}} \geq \tau_{i,j}, \quad \text{for } j = 1, \cdots, 2^{N_r} - 1,\ i = 1, \cdots, W_j, \tag{36}$$

$$(9),\ (10),\ \text{and}\ (11).$$

The equivalence between (P2) and (P2.1) can be easily verified since the constraint in (36) holds with equality at the optimal. Otherwise, we can always increase $\tau_{i,j}$ without decreasing the objective value.

Still, (P2.1) is a non-convex problem in general due to the constraint in (35). To address this issue, we adopt the SCA technique [31] which iteratively solves a sequence of approximated convex problems for the original non-convex one. It has been known that with proper approximations, the SCA algorithm converges to a locally optimal solution

of the original non-convex problem. In each iteration of the SCA algorithm, we need to construct a surrogate function of the non-convex constraint (35) which provides a concave lower bound of $\Xi(\delta_j, \tau_{i,j})$ [25]. The following lemma presents a tractable surrogate function $\Xi_{LB}^{(l)}(\delta_j, \tau_{i,j})$ for the function $\Xi(\delta_j, \tau_{i,j})$.

Lemma 3: Let us denote $\delta^{(l)}$ and $\tau^{(l)}$ as solutions for δ and τ obtained at the l-th iteration of the SCA algorithm, respectively. Then, the concave surrogate function $\Xi_{LB}^{(l)}(\delta_j, \tau_{i,j})$ for $\Xi(\delta_j, \tau_{i,j})$ can be expressed as

$$\Xi_{LB}^{(l)}(\delta_j, \tau_{i,j}) \triangleq \chi \frac{\tau_{i,j}^2}{\delta_j} + \kappa_1\left(\delta_j^{(l)}, \tau_{i,j}^{(l)}\right)\tau_{i,j} + \kappa_2\left(\delta_j^{(l)}, \tau_{i,j}^{(l)}\right)\delta_j \leq \Xi(\delta_j, \tau_{i,j}),$$

where

$$\kappa_1\left(\delta_j^{(l)}, \tau_{i,j}^{(l)}\right) \triangleq \frac{a\exp\left(ab + a\frac{\tau_{i,j}^{(l)}}{\delta_j^{(l)}}\right)}{\left(\exp(ab) + \exp\left(a\frac{\tau_{i,j}^{(l)}}{\delta_j^{(l)}}\right)\right)^2} - 2\chi\frac{\tau_{i,j}^{(l)}}{\delta_j^{(l)}},$$

$$\kappa_2\left(\delta_j^{(l)}, \tau_{i,j}^{(l)}\right) \triangleq \chi\left(\frac{\tau_{i,j}^{(l)}}{\delta_j^{(l)}}\right)^2 - \frac{a\tau_{i,j}^{(l)}\exp\left(ab + a\frac{\tau_{i,j}^{(l)}}{\delta_j^{(l)}}\right)}{\delta_j^{(l)}\left(\exp(ab) + \exp\left(a\frac{\tau_{i,j}^{(l)}}{\delta_j^{(l)}}\right)\right)^2} + \frac{1}{1 + \exp\left(-a\frac{\tau_{i,j}^{(l)}}{\delta_j^{(l)}} + ab\right)} - c,$$

with $\chi \triangleq -\frac{a^2(5+3\sqrt{3})}{54+30\sqrt{3}} = -0.0481a^2 < 0$.

Proof: See Appendix C. ∎

With the aid of Lemma 3, at the $(l+1)$-th iteration of the SCA procedure, we can express a convex approximation of (P2.1) as

$$\text{(P2.2)} \quad \max_{\substack{\{\hat{\mathbf{Q}}_j \succeq 0\}, \{\delta_j \geq 0\} \\ \{\tau_{i,j} \geq 0\}}} \sum_{j=2}^{2^{N_r}} \delta_j \log\left|\mathbf{I}_{M_j} + \frac{1}{\delta_j}\mathbf{H}_j\hat{\mathbf{Q}}_j\mathbf{H}_j^H\right|$$
$$\text{s.t.} \sum_{j=1}^{2^{N_r}-1}\sum_{i=1}^{W_j}\Xi_{LB}^{(l)}(\delta_j, \tau_{i,j}) \geq \frac{(1-c)\bar{E}}{M},$$
$$(9),\ (10),\ (11),\ \text{and}\ (36).$$

As a result, (P2.2) can be optimally solved via existing convex optimization solvers, e.g., CVX [27]. Finally, we summarize an iterative procedure for (P2) in Algorithm 3 as below. Since the proposed surrogate function $\Xi_{LB}^{(l)}(\delta_j, \tau_{i,j})$ fulfills the conditions in [31], it is guaranteed that Algorithm 3 converges to at least a locally optimal point [25], [31]. Notice that the proposed antenna mode selection method in Section III-C can also be applied to the non-linear EH model along with Algorithm 3. For the initialization of Algorithm 3, we set $\delta_j^{(0)} = \frac{1}{2^{N_r}}$ and $\tau_{i,j}^{(0)} = 10^{-3}$, $\forall i, j$.[5]

[5]We confirm through our simulation that this simple initialization is sufficient for achieving good performance.

Algorithm 3 Proposed Algorithm for Solving (P2)

Initialize $l = 0$, $\{\delta_j^{(l)}\}$, and $\{\tau_{i,j}^{(l)}\}$, $\forall i, j$.
Repeat
Solve (P2.2) with given $\{\delta_j^{(l)}\}$ and $\{\tau_{i,j}^{(l)}\}$ and obtain the solution $\{\delta_j^{(l+1)}\}$ and $\{\tau_{i,j}^{(l+1)}\}$.
Update $l \leftarrow l + 1$.
Until convergence.

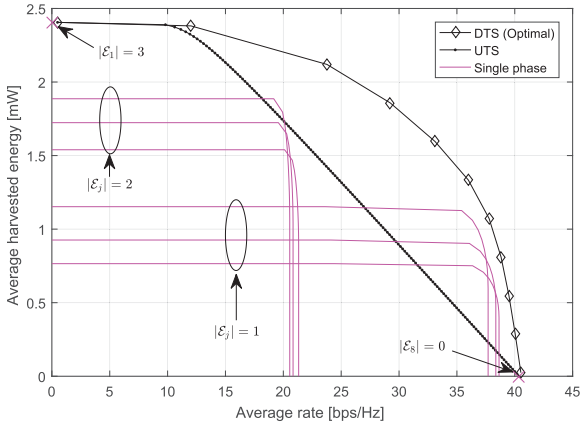

Fig. 4. Average R-E region of the linear EH model with $N_t = 2$ and $N_r = 3$.

V. Simulation Results

In this section, we present numerical results to validate the proposed DTS protocol. The peak power constraint is set as $P_P = 1.5P_A$ and the noise variance at the receiver is given by $\sigma^2 = -60$ dBm. Unless specified otherwise, the power budget at the transmitter and the EH efficiency are assumed to be $P_A = 30$ dB and $\eta = 0.4$, respectively. For the non-linear EH model, the constants M, a, and b are set to be $M = 2.8$ mW, $a = 1500$, and $b = 0.0022$, respectively [20], [24]. All the simulation results obtained in this section are averaged over Rayleigh fading channel realizations with the average pathloss of 30 dB.

In Fig. 4, we illustrate the average R-E region of the proposed DTS protocol for the linear EH model with $N_t = 2$ and $N_r = 3$. For comparison, the R-E region of conventional UTS and "Single phase" schemes are also plotted. Here, the "Single phase" represents a simple SWIPT system where only a single phase is selected out of total 2^{N_r} phases of the proposed DTS protocol. Thus, in the "Single phase" scheme, the received signals at antennas $\mathcal{E}_k$ are used for the EH, while those at $\mathcal{I}_k$ are utilized for the ID during one system frame. From this figure, the achievable harvested energy region of the "Single phase" gets larger as the number of EH antennas $|\mathcal{E}_k|$ increases, and this is attributed to the fact that $\lambda_{\mathbf{G}_k,1}$ becomes higher as $|\mathcal{E}_k|$ grows in general. It is worth noting that the proposed DTS exhibits a much larger R-E region than other schemes. Hence, it is identified that the time durations as well as the precoding matrices for the multiple modes should be carefully optimized to improve the SWIPT performance.

Fig. 5 exhibits the average R-E region of the proposed DTS and the conventional UTS scheme of the linear EH model for

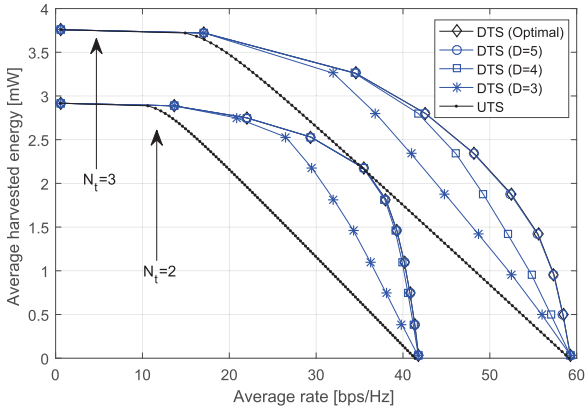

Fig. 5. Average R-E region of the linear EH model for $N_t = 2$ and 3 with $N_r = 4$.

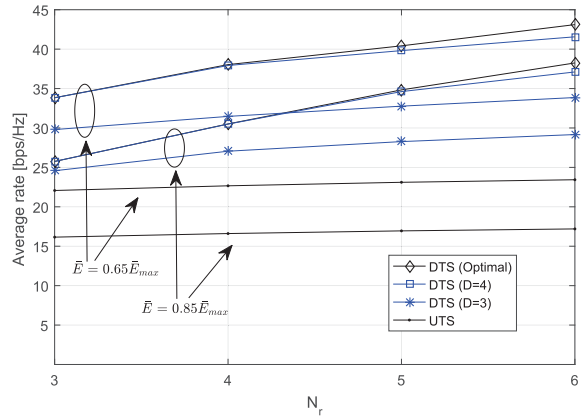

Fig. 6. Average rate performance for the linear EH model as a function of N_r with $\bar{E} = 0.85\bar{E}_{max}$ and $0.65\bar{E}_{max}$.

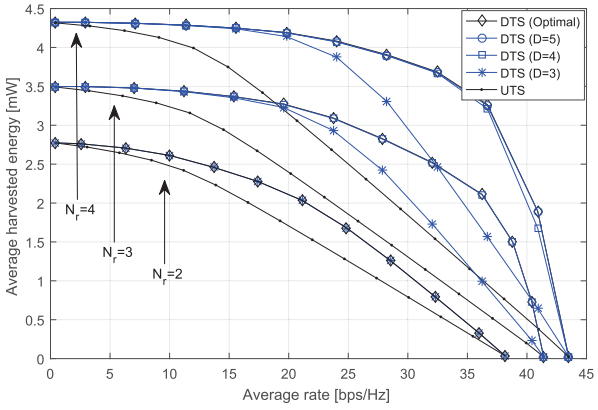

Fig. 7. Average R-E region of the non-linear EH model for $N_r = 2$, 3, and 4 with $N_t = 2$.

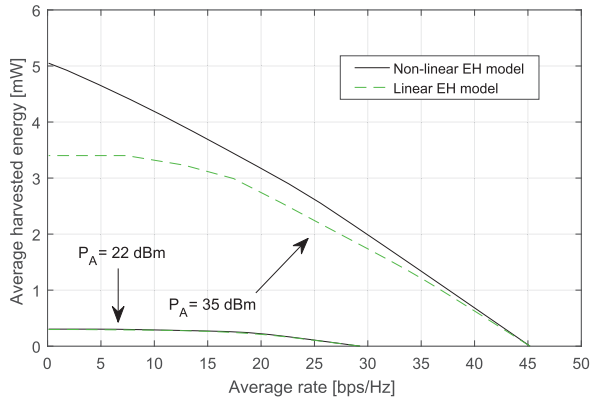

Fig. 8. Comparison between the linear and non-linear EH models with $N_t = N_r = 2$ and $P_A = 23$dBm and 35dBm.

$N_t = 2$ and 3 with $N_r = 4$. To investigate the impact of the proposed low-complexity antenna mode selection method, the performance of the DTS is evaluated for different number of antenna sets D. For the optimal DTS, the transceiver optimization in Algorithm 1 is applied, while for $D < 2^{N_r}$, the antenna selection method in Section III-C is performed. From the figure, we can see that the proposed DTS generates larger R-E regions than the conventional UTS for all N_t and D. This is because the conventional UTS is a special case of the DTS protocol with $D = 2$. Also, it is observed that the DTS with $D = 5$ achieves the near optimal performance of $D = 2^4$, which demonstrates the efficacy of the proposed antenna selection method. Note that a complexity reduction of the antenna selection algorithm with $D = 5$ is 96.44% compared to the optimal DTS.

Fig. 6 depicts the average rate performance of the linear EH model as a function of the number of receive antennas N_r with $N_t = 2$ for the EH constraints $\bar{E} = 0.65\bar{E}_{max}$ and $0.85\bar{E}_{max}$. Again, it can be verified that the proposed DTS outperforms the conventional UTS scheme for all simulated $\bar{E}$. In particular, the performance gap between the two methods increases as N_r grows, since the degree of freedom for the DTS protocol design becomes higher. When $\bar{E} = 0.85\bar{E}_{max}$, the average rate performance gains of the proposed DTS over the conventional UTS are about 60 % and 122 % for $N_r = 3$ and 6, respectively. In addition, when the proposed antenna mode selection is employed for the DTS with $D = 4$, a performance loss becomes negligible compared to the optimal DTS. These results confirm the effectiveness of our DTS protocol.

Next, in Fig. 7, we plot the average R-E region of the non-linear EH model for $N_r = 2$, 3, and 4 with $N_t = 2$. As seen in this figure, the average R-E regions of all schemes become larger as the number of receive antennas grows. Similar to the linear EH model case, the optimal DTS exhibits the largest average R-E region, while the conventional UTS shows the worst SWIPT performance. Also, it is obvious that the proposed antenna selection method with $D = 5$ achieves almost the same R-E region with the optimal one when $N_r = 4$. This infers that our low-complexity design approach is able to offer the performance very close to the optimum.

Fig. 8 compares the performance for the linear and non-linear EH models in Algorithms 1 and 3, respectively, with $N_t = N_r = 2$, $D = 2^{N_r} = 4$, and $\eta = 0.7$ for $P_A = 23$ dBm and 35 dBm. Here, the average R-E region is evaluated under the non-linear EH model, i.e., we obtain (6) by substituting $\{\mathbf{Q}_j^\star\}$ and $\{\delta_j^\star\}$ computed via Algorithm 1 for the linear EH case. First, it is checked that for $P_A = 35$ dBm, the proposed

algorithm for the non-linear EH model generates much larger R-E region than that for the linear EH model, since the mismatch between the linear model and the measurement data is large in the high input RF power regime as illustrated in Fig. 3. However, two algorithms exhibit similar performance when $P_A = 23$ dBm, indicating that the linear EH model is accurate if the average transmit power at the transmitter is small. Notice that the proposed algorithm for the linear EH model is more computationally efficient than that for the non-linear model. Thus, for the low P_A regime, we can employ Algorithm 1 for the linear EH model in practice to achieve proper SWIPT performance with lower complexity.

VI. Conclusion

In this paper, we have proposed the DTS protocol in the P2P SWIPT MIMO systems for both linear and non-linear EH models. The proposed DTS can be viewed as a general framework for the TS-based SWIPT schemes and includes the conventional UTS method as a special case. To fully identify the performance of the DTS protocol, we focus on the achievable R-E region by solving the rate maximization problems under the EH constraint. For a low-complexity algorithm, an antenna mode selection method has also been proposed which achieves near-optimal performance with much reduced complexity. Numerical results have demonstrated the effectiveness of the DTS scheme. This paper has focused on the investigation of the theoretical performance of the proposed DTS architecture. Practical implementation issues of the DTS protocol such as an extension to massive MIMO configurations and the performance optimization with imperfect CSI would be important future research plans. A performance comparison between the DTS and the dynamic PS protocols with multiple EH circuits is worth pursuing as a future work.

Appendix A
Proof of Lemma 1

For $\delta_j = 0$, one can easily identify that from the peak power constraint (26), the optimal $\tilde{\mathbf{Q}}_j^\star$ becomes a zero matrix. Consequently, we consider a non-trivial case of $\delta_j > 0$ for $j = 1, \cdots, 2^{N_r}$. The problem in (24) is convex and satisfies the Slater's condition, and thus the duality gap is zero [27]. Hence, it can be optimally solved by employing the Lagrange duality method. First, it is straightforward to show that the optimal $\tilde{\mathbf{Q}}_{2^{N_r}}^\star$ for (24) equals $\tilde{\mathbf{Q}}_{2^{N_r}}^\star = \mathbf{0}$ since $\tilde{E}\left(\{\delta_j\}\right)$ is independent of $\tilde{\mathbf{Q}}_{2^{N_r}}$.

Next, to compute the optimal solution $\tilde{\mathbf{Q}}_j^\star$ for $j = 1, \cdots, 2^{N_r} - 1$, the KKT conditions for problem (24) are rewritten as

$$\left(\mathbf{G}_j^H \mathbf{G}_j - (\phi^\star + \theta_j^\star)\mathbf{I}_{N_t}\right)\tilde{\mathbf{Q}}_j^\star = \mathbf{0}, \quad \forall j, \tag{37}$$

$$(\phi^\star + \theta_j^\star)\mathbf{I}_{N_t} - \mathbf{G}_j^H \mathbf{G}_j \succeq 0, \quad \forall j, \tag{38}$$

$$\phi^\star \left(P_A - \sum_{j=1}^{2^{N_r}-1} \mathrm{tr}(\tilde{\mathbf{Q}}_j^\star)\right) = 0, \tag{39}$$

$$\theta_j^\star \left(P_P \delta_j - \mathrm{tr}(\tilde{\mathbf{Q}}_j^\star)\right) = 0, \quad \forall j, \tag{40}$$

where $\phi^\star$ and $\{\theta_j^\star\}$ are the optimal dual variables, (38) comes from the fact that $\tilde{E}\left(\{\delta_j\}\right)$ must have a bounded value, and (39) and (40) indicate the complementary slackness conditions. Note that (38) can be equivalently expressed as[6]

$$\phi^\star + \theta_j^\star \geq \lambda_{\mathbf{G}_j,1} > 0, \quad \forall j. \tag{41}$$

In what follows, we investigate (41) for two different cases $\phi^\star = 0$ and $\phi^\star > 0$. For the first case of $\phi^\star = 0$, from (41), the optimal dual variable $\theta_j^\star$ is bounded as $\theta_j^\star \geq \lambda_{\mathbf{G}_j,1} > 0, \forall j$. When $\theta_j^\star > \lambda_{\mathbf{G}_j,1}$, we have $\tilde{\mathbf{Q}}_j^\star = \mathbf{0}$ by employing (37), which violates the complementary condition (40). Accordingly, for $\phi^\star = 0$, the optimal $\theta_j^\star$ is calculated by $\theta_j^\star = \lambda_{\mathbf{G}_j,1}$, and the corresponding optimal transmit covariance matrix $\tilde{\mathbf{Q}}_j^\star$ from (37) and (40) is written as

$$\tilde{\mathbf{Q}}_j^\star = P_P \delta_j \mathbf{v}_{\mathbf{G}_j,1} \mathbf{v}_{\mathbf{G}_j,1}^H, \quad \forall j. \tag{42}$$

By substituting (42) into the sum power constraint in (25), it can be verified that the case of $\phi^\star = 0$ corresponds to $\sum_{j=1}^{2^{N_r}-1} \delta_j \leq \frac{P_A}{P_P}$.

Now, we consider the case where the optimal $\phi^\star$ is a positive number, which only occurs when $\sum_{j=1}^{2^{N_r}-1} \delta_j > \frac{P_A}{P_P}$ with $\theta_j^\star = 0$ for some j. Let us define $\mathcal{P}$ as the set of phase indices j such that $\theta_j^\star > 0$. For $j \in \mathcal{P}$, it should follow $\phi^\star + \theta_j^\star = \lambda_{\mathbf{G}_j,1}$ from (41), since otherwise when $\phi^\star + \theta_j^\star > \lambda_{\mathbf{G}_j,1}$, the optimal $\tilde{\mathbf{Q}}_j^\star$ is not feasible similar to the first case of this proof. Therefore, we always obtain $\phi^\star + \theta_j^\star = \lambda_{\mathbf{G}_j,1}$ for $j \in \mathcal{P}$, which leads to the optimal matrix $\tilde{\mathbf{Q}}_j^\star = P_P \delta_j \mathbf{v}_{\mathbf{G}_j,1} \mathbf{v}_{\mathbf{G}_j,1}^H$.

Next, for $j \in \mathcal{P}^c$, we have $\phi^\star \geq \lambda_{\mathbf{G}_j,1}$. If $\phi^\star > \lambda_{\mathbf{G}_j,1}$, the optimal $\tilde{\mathbf{Q}}_j^\star$ is given by $\tilde{\mathbf{Q}}_j^\star = \mathbf{0}$ due to the condition in (37). On the other hand, there exists at most one $j \in \mathcal{P}^c$ for $\phi^\star = \lambda_{\mathbf{G}_j,1}$, and the optimal solution $\tilde{\mathbf{Q}}_j^\star$ can be computed from (39) as $\tilde{\mathbf{Q}}_j^\star = d \mathbf{v}_{\mathbf{G}_j,1} \mathbf{v}_{\mathbf{G}_j,1}^H$ with $d \in [0, P_P \delta_j]$ satisfying $\sum_{j=1}^{2^{N_r}-1} \mathrm{tr}(\tilde{\mathbf{Q}}_j^\star) = P_A$. Without loss of generality, suppose that the phases are sorted such that $\lambda_{\mathbf{G}_j,1} > \lambda_{\mathbf{G}_k,1}$ for $j < k$. Recalling the facts $\phi^\star + \theta_j^\star = \lambda_{\mathbf{G}_j,1}$ for $j \in \mathcal{P}$ and $\phi^\star \geq \lambda_{\mathbf{G}_j,1}$ for $j \in \mathcal{P}^c$, we have

$$\max_{j \in \mathcal{P}^c} \lambda_{\mathbf{G}_j,1} \leq \phi^\star < \min_{j \in \mathcal{P}} \lambda_{\mathbf{G}_j,1}.$$

Then, there always exists a unique phase index $N \in \mathcal{P}^c$ such that

$$\lambda_{\mathbf{G}_{2^{N_r}-1},1} < \cdots < \lambda_{\mathbf{G}_N,1} \leq \phi^\star < \lambda_{\mathbf{G}_{N-1},1} < \cdots < \lambda_{\mathbf{G}_1,1}.$$

Hence, the set $\mathcal{P}$ is identified as $\mathcal{P} = \{1, \cdots, N-1\}$. Based on these results, the optimal covariance matrix becomes $\tilde{\mathbf{Q}}_j^\star = \zeta_j \mathbf{v}_{\mathbf{G}_j,1} \mathbf{v}_{\mathbf{G}_j,1}^H$, where

$$\zeta_j = \begin{cases} P_P \delta_j, & \text{for } j = 1, \cdots, N-1, \\ P_A - \sum_{j=1}^{N-1} \mathrm{tr}(\tilde{\mathbf{Q}}_j^\star), & \text{for } j = N, \\ 0, & \text{for } j = N+1, \cdots, 2^{N_r}-1. \end{cases} \tag{43}$$

We can check that N is the minimum index n satisfying $\sum_{j=1}^{n} \delta_j > \frac{P_A}{P_P}$. Plugging (43) into the objective in (24), we complete the proof.

[6] In the random fading environment, the channel matrices are not orthogonal to each other in general, and thus the eigenvalues $\{\lambda_{\mathbf{G}_j,1}\}$ are not the same, i.e., $\lambda_{\mathbf{G}_j,1} \neq \lambda_{\mathbf{G}_i,1}$ for $j \neq i$, with probability one.

APPENDIX B
PROOF OF LEMMA 2

For notational simplicity, we define $\boldsymbol{\delta} = [\delta_1, \cdots, \delta_{2^{N_r}}]$. To prove the concavity of $\tilde{E}(\boldsymbol{\delta})$, we first show that its domain $\mathcal{K} = \bigcup_{N=1}^{2^{N_r}} \mathcal{D}_N$ is a convex set, where

$$\mathcal{D}_N = \left\{ \boldsymbol{\delta} \left| \frac{P_A}{P_P} < \sum_{j=1}^{N} \delta_j \leq \frac{P_A}{P_P} + \delta_N \right. \right\}. \tag{44}$$

Suppose that feasible solutions $\boldsymbol{\delta}^1$ and $\boldsymbol{\delta}^2$ satisfy $\boldsymbol{\delta}^1 \in \mathcal{D}_{N_1}$ and $\boldsymbol{\delta}^2 \in \mathcal{D}_{N_2}$, respectively, for integers $N_1, N_2 \in [1, 2^{N_r}]$. Then, if there exists an integer $N_3 \in [1, 2^{N_r}]$ such that $\boldsymbol{\delta}^3 \triangleq \theta\boldsymbol{\delta}^1 + (1-\theta)\boldsymbol{\delta}^2 \in \mathcal{D}_{N_3} \subset \mathcal{K}$ for all $0 \leq \theta \leq 1$, we can show that the feasible set $\mathcal{K}$ is convex.

We consider two different cases where $N_1 = N_2$ and $N_1 < N_2$. First, when $N_1 = N_2$, it is easy to verify that for all $0 \leq \theta \leq 1$, $\boldsymbol{\delta}^3$ is always in the set $\mathcal{D}_{N_1}$ since

$$\sum_{j=1}^{N_1-1} \left(\theta\delta_j^1 + (1-\theta)\delta_j^2\right) \leq \theta\frac{P_A}{P_P} + (1-\theta)\frac{P_A}{P_P} = \frac{P_A}{P_P},$$
$$\sum_{j=1}^{N_1} \left(\theta\delta_j^1 + (1-\theta)\delta_j^2\right) > \theta\frac{P_A}{P_P} + (1-\theta)\frac{P_A}{P_P} = \frac{P_A}{P_P}.$$

Similarly, for the second case with $N_1 < N_2$, we can always find an integer $N_3 \in [1, 2^{N_r}]$ such that $N_1 \leq N_3 \leq N_2$ and $\boldsymbol{\delta}^3 \in \mathcal{D}_{N_3}$. Thus, the feasible domain of $\tilde{E}(\boldsymbol{\delta})$ is a convex set.

Now, we investigate the concavity of $\tilde{E}(\boldsymbol{\delta})$ by proving

$$\tilde{E}\big(\boldsymbol{\delta}^3\big) \geq \theta\tilde{E}\big(\boldsymbol{\delta}^1\big) + (1-\theta)\tilde{E}\big(\boldsymbol{\delta}^2\big), \tag{45}$$

for $\boldsymbol{\delta}^k \in \mathcal{D}_{N_k}$ and $k = 1, 2, 3$. In the first case of $N_1 = N_2$, since $N_3 = N_1$, we can easily identify that (45) always holds with the equality. Next, we examine the second case where $N_1 \leq N_3 \leq N_2$. Let us define a function $A_N(\boldsymbol{\delta})$ as

$$A_N\big(\boldsymbol{\delta}\big) = P_P \sum_{j=1}^{N-1} \lambda_{\mathbf{G}_j,1}\delta_j + \left(P_A - P_P \sum_{j=1}^{N-1} \delta_j\right) \lambda_{\mathbf{G}_N,1}.$$

To show (45), we first verify the fact that $\tilde{E}\big(\hat{\boldsymbol{\delta}}\big) < A_{N-n}\big(\hat{\boldsymbol{\delta}}\big)$ always holds for any $\hat{\boldsymbol{\delta}} \in \mathcal{D}_N$ and an integer $0 < n < N$.

It follows

$$\begin{aligned}
&\tilde{E}\big(\hat{\boldsymbol{\delta}}\big) - A_{N-n}\big(\hat{\boldsymbol{\delta}}\big) \\
&\quad = P_P\left(\lambda_{\mathbf{G}_{N-n},1} - \lambda_{\mathbf{G}_N,1}\right)\left(\sum_{j=1}^{N-n-1} \hat{\delta}_j - \frac{P_A}{P_P}\right) \\
&\qquad + P_P \sum_{j=N-n}^{N-1} \left(\lambda_{\mathbf{G}_j,1} - \lambda_{\mathbf{G}_N,1}\right)\hat{\delta}_j \\
&\quad < P_P\left(\lambda_{\mathbf{G}_{N-n},1} - \lambda_{\mathbf{G}_N,1}\right)\left(\sum_{j=1}^{N-1} \hat{\delta}_j - \frac{P_A}{P_P}\right) \qquad (46) \\
&\quad \leq 0, \qquad (47)
\end{aligned}$$

where (46) and (47) respectively come from the facts $\lambda_{\mathbf{G}_j,1} > \lambda_{\mathbf{G}_k,1}$ for $j < k$ and $\hat{\boldsymbol{\delta}} \in \mathcal{D}_N$.

Also, we can show $\tilde{E}\big(\hat{\boldsymbol{\delta}}\big) < A_{N+n}\big(\hat{\boldsymbol{\delta}}\big)$ as

$$\begin{aligned}
&\tilde{E}\big(\hat{\boldsymbol{\delta}}\big) - A_{N+n}\big(\hat{\boldsymbol{\delta}}\big) \\
&\quad = P_P\left(\lambda_{\mathbf{G}_N,1} - \lambda_{\mathbf{G}_{N+n},1}\right)\left(\frac{P_A}{P_P} - \sum_{j=1}^{N} \hat{\delta}_j\right) \\
&\qquad - P_P \sum_{j=N+1}^{N+n-1} \left(\lambda_{\mathbf{G}_j,1} - \lambda_{\mathbf{G}_{N+n},1}\right)\hat{\delta}_j \\
&\quad < 0. \qquad (48)
\end{aligned}$$

Repeatedly, $\tilde{E}\big(\boldsymbol{\delta}\big)$ is an affine function for all N. Therefore, by using (47) and (48), we have

$$\begin{aligned}
\tilde{E}\big(\boldsymbol{\delta}^3\big) &= \theta A_{N_3}\big(\boldsymbol{\delta}^1\big) + (1-\theta)A_{N_3}\big(\boldsymbol{\delta}^2\big) \\
&> \theta\tilde{E}\big(\boldsymbol{\delta}^1\big) + (1-\theta)\tilde{E}\big(\boldsymbol{\delta}^2\big),
\end{aligned}$$

which concludes that $\tilde{E}(\boldsymbol{\delta})$ is a concave function.

APPENDIX C
PROOF OF LEMMA 3

Let us rewrite the function $\Xi(\delta_j, \tau_{i,j})$ as $\Xi(\delta_j, \tau_{i,j}) = \delta_j\Psi\left(\frac{\tau_{i,j}}{\delta_j}\right)$, where $\Psi(x) \triangleq \frac{1}{1+\exp(-ax+ab)} - c$. To derive the surrogate function of $\Xi(\delta_j, \tau_{i,j})$, we first focus on $\Psi(x)$ which is non-decreasing and has a bounded curvature. For any given local point $x^{(l)}$, a lower bound $\Psi_{LB}^{(l)}(x)$ of the function $\Psi(x)$ is given by

$$\begin{aligned}
\Psi(x) &\geq \frac{\chi}{2}\left(x - x^{(l)}\right)^2 + \frac{\partial\Psi(x^{(l)})}{\partial x}\left(x - x^{(l)}\right) + \Psi\big(x^{(l)}\big) \\
&\triangleq \Psi_{LB}^{(l)}(x). \qquad (49)
\end{aligned}$$

To construct the lower bound in (49), the constant χ is chosen to satisfy $\chi \leq \frac{\partial^2\Psi(x)}{\partial x^2}$ for any positive number x [31]. Thus, we need to find the minimum value of $\frac{\partial^2\Psi(x)}{\partial x^2}$ with respect to $x \geq 0$.

The third order derivative of $\Psi(x)$ can be attained by

$$\begin{aligned}
\frac{\partial^3\Psi(x)}{\partial x^3} = &\frac{\left(\exp(2ab) + \exp(2ax) - 4\exp(a(b+x))\right)}{\left(\exp(ab) + \exp(ax)\right)^4} \\
&\times a^3\exp(a(b+x)). \qquad (50)
\end{aligned}$$

By solving the equation $\frac{\partial^3\Psi(x)}{\partial x^3} = 0$, the stationary points of $\frac{\partial^3\Psi(x)}{\partial x^3}$ can be computed as $x_1 = \frac{1}{a}\ln(2-\sqrt{3}) + b$ and $x_2 = \frac{1}{a}\ln(2+\sqrt{3}) + b$. From (50), it can be verified that $\frac{\partial^3\Psi(x)}{\partial x^3}$ is positive for $0 \leq x < x_1$ and $x > x_2$, while $\frac{\partial^3\Psi(x)}{\partial x^3}$ is negative for $x_1 < x < x_2$, which implies that $\frac{\partial^2\Psi(x)}{\partial x^2}$ achieves the minimum at $x = x_2$. Hence, χ in (49) is calculated as $\chi = -\frac{a^2(5+3\sqrt{3})}{54+30\sqrt{3}}$.

Now, we consider the function $\Xi(\delta_j, \tau_{i,j}) = \delta_j\Psi\left(\frac{\tau_{i,j}}{\delta_j}\right)$, whose lower bound $\Xi_{LB}^{(l)}(\delta_j, \tau_{i,j})$ can be obtained from (49) as $\Xi_{LB}^{(l)}(\delta_j, \tau_{i,j}) = \delta_j\Psi_{LB}^{(l)}\left(\frac{\tau_{i,j}}{\delta_j}\right)$. Provided that $\chi < 0$, one can easily check that $\Psi_{LB}^{(l)}(x)$ is a concave function. Thus, the function $\Xi_{LB}^{(l)}(\delta_j, \tau_{i,j})$, which is the perspective of $\Psi_{LB}^{(l)}(x)$, is also concave, since the perspective operation guarantees the concavity [27]. Also, we can prove

the facts $\Xi_{LB}^{(l)}(\delta_j^{(l)},\tau_{i,j}^{(l)}) = \Xi(\delta_j^{(l)},\tau_{i,j}^{(l)})$, $\frac{\partial \Xi_{LB}^{(l)}(\delta_j^{(l)},\tau_{i,j}^{(l)})}{\partial \delta_j} = \frac{\partial \Xi(\delta_j^{(l)},\tau_{i,j}^{(l)})}{\partial \delta_j}$, and $\frac{\partial \Xi_{LB}^{(l)}(\delta_j^{(l)},\tau_{i,j}^{(l)})}{\partial \tau_{i,j}} = \frac{\partial \Xi(\delta_j^{(l)},\tau_{i,j}^{(l)})}{\partial \tau_{i,j}}$, which indicate that $\Xi_{LB}^{(l)}(\delta_j^{(l)},\tau_{i,j}^{(l)})$ is a surrogate function of $\Xi(\delta_j^{(l)},\tau_{i,j}^{(l)})$ [25]. This completes the proof.

REFERENCES

[1] P. Nintanavongsa, U. Muncuk, D. R. Lewis, and K. R. Chowdhury, "Design optimization and implementation for RF energy harvesting circuits," *IEEE J. Emerg. Sel. Topics Circuits Syst.*, vol. 2, no. 1, pp. 24–33, Mar. 2012.

[2] H. Lee, K.-J. Lee, H. Kim, B. Clerckx, and I. Lee, "Resource allocation techniques for wireless powered communication networks with energy storage constraint," *IEEE Trans. Wireless Commun.*, vol. 15, no. 4, pp. 2619–2628, Apr. 2016.

[3] H. Kim, H. Lee, M. Ahn, H.-B. Kong, and I. Lee, "Joint subcarrier and power allocation methods in full duplex wireless powered communication networks for OFDM systems," *IEEE Trans. Wireless Commun.*, vol. 15, no. 7, pp. 4745–4753, Jul. 2016.

[4] R. Zhang, and C. K. Ho, "MIMO broadcasting for simultaneous wireless information and power transfer," *IEEE Trans. Wireless Commun.*, vol. 12, no. 5, pp. 1989–2001, May 2013.

[5] H. Lee, S.-R. Lee, K.-J. Lee, H.-B. Kong, and I. Lee, "Optimal beamforming designs for wireless information and power transfer in MISO interference channels," *IEEE Trans. Wireless Commun.*, vol. 14, no. 9, pp. 4810–4821, Sep. 2015.

[6] S. Kang, H.-B. Kong, C. Song, H. Lee, and I. Lee, "Transmit probability designs for wireless peer discovery with energy harvesting," *IEEE Commun. Lett.*, vol. 21, no. 3, pp. 644–647, Mar. 2017.

[7] Z. Zong, H. Feng, F. R. Yu, N. Zhao, T. Yang, and B. Hu, "Optimal transceiver design for SWIPT in K-user MIMO interference channels," *IEEE Trans. Wireless Commun.*, vol. 15, no. 1, pp. 430–445, Jan. 2016.

[8] H. Lee, C. Song, S.-H. Choi, and I. Lee, "Outage probability analysis and power splitter designs for SWIPT relaying systems with direct link," *IEEE Commun. Lett.*, vol. 21, no. 3, pp. 648–651, Mar. 2017.

[9] A. Karminezhad, S. Gherekhloo, and A. Sezgin, "Optimal power splitting for simultaneous information detection and energy harvesting," *IEEE Signal Process. Lett.*, vol. 24, no. 7, pp. 963–967, Jul. 2017.

[10] S. Li, W. Xu, Z. Liu, and J. Lin, "Independent power splitting for interference-corrupted SIMO SWIPT systems," *IEEE Commun. Lett.*, vol. 20, no. 3, pp. 478–481, Mar. 2016.

[11] C. Shen, W.-C. Li, and T.-H. Chang, "Wireless information and energy transfer in multi-antenna interference channel," *IEEE Trans. Signal Process.*, vol. 62, no. 23, pp. 6249–6264, Dec. 2014.

[12] H. Yu, Y. Zhang, S. Guo, Y. Yang, and L. Ji, "Energy efficiency maximization for WSNs with simultaneous wireless informaion and power transfer," *Sensors*, vol. 17, no. 7, pp. 1524–1537, Jul. 2017.

[13] Q. Gu, G. Wang, R. Fan, Z. Zhong, K. Yang, and H. Jiang, "Rate-energy tradeoff in simultaneous wireless information and power transfer over fading channels with uncertain distribution," *IEEE Trans. Veh. Technol.*, vol. 67, no. 4, pp. 3663–3668, Apr. 2018.

[14] L. Ma, Y. Wang, and Y. Xu, "Sum rate optimization for SWIPT system based on zero-forcing beamforming and time switching," in *Proc. IEEE IWCMC*, Jun. 2017, pp. 351–356.

[15] S. Salari, I.-M. Kim, D. I. Kim, and F. Chan, "Joint EH time allocation and distributed beamforming in interference-limited two-way networks with EH-based relays," *IEEE Trans. Wireless Commun.*, vol. 16, no. 10, pp. 6395–6408, Oct. 2017.

[16] J. Liao, M. R. A. Khandaker, and K.-K. Wong. (2017). "Energy harvesting enabled MIMO relaying through time switching." [Online]. Available: https://arxiv.org/abs/1704.02907

[17] J. Tang, D. K. C. So, N. Zhao, A. Shojaeifard, and K.-K. Wong, "Energy efficiency optimization with SWIPT in MIMO broadcast channels for Internet of Things," *IEEE Internet Things J.*, vol. 5, no. 4, pp. 2605–2619, Aug. 2018.

[18] N. Janatian, I. Stupia, and L. Vandendorpe, "Joint multi-objective transmit precoding and receiver time switching design for MISO SWIPT systems," in *Proc. IEEE 17th Int. Workshop Signal Process. Adv. Wireless Commun. (SPAWC)*, Jul. 2016, pp. 1–5.

[19] K. Xiong, B. Wang, and K. J. R. Liu, "Rate-energy region of SWIPT for MIMO broadcasting under nonlinear energy harvesting model," *IEEE Trans. Commun.*, vol. 16, no. 8, pp. 5147–5161, Aug. 2017.

[20] J. Guo, H. Zhang, and X. Zhu, "Theoretical analysis of RF-DC conversion efficiency for class-F rectifiers," *IEEE Trans. Microw. Theory Techn.*, vol. 62, no. 4, pp. 977–985, Apr. 2014.

[21] D. Mishra, S. De, and D. Krishnaswamy, "Dilemma at RF energy harvesting relay: Downlink energy relaying or uplink information transfer?" *IEEE Trans. Wireless Commun.*, vol. 16, no. 8, pp. 4939–4955, Aug. 2017.

[22] E. Boshkovska, D. W. K. Ng, N. Zlatanov, and R. Schober, "Practical non-linear energy harvesting model and resource allocation for SWIPT systems," *IEEE Commun. Lett.*, vol. 19, no. 12, pp. 2082–2085, Dec. 2015.

[23] R. Jiang, K. Xiong, P. Fan, Y. Zhang, and Z. Zhong, "Optimal design of SWIPT systems with multiple heterogeneous users under non-linear energy harvesting model," *IEEE Access*, vol. 5, pp. 11479–11489, Jul. 2017.

[24] K. Xiong, B. Wang, and K. J. R. Liu, "Rate-energy region of SWIPT for MIMO broadcasting under nonlinear energy harvesting model," *IEEE Trans. Wireless Commun.*, vol. 16, no. 8, pp. 5147–5161, Aug. 2017.

[25] B. R. Marks and G. P. Wright, "A general inner approximation algorithm for nonconvex mathematical programs," *Oper. Res.*, vol. 26, no. 4, pp. 681–683, Jul. 1978.

[26] C. Psomas and I. Krikidis, "A wireless powered feedback protocol for opportunistic beamforming using rectenna arrays," *IEEE Trans. Green Commun. Netw.*, vol. 2, no. 1, pp. 100–113, Mar. 2018.

[27] S. Boyd and L. Vandenberghe, *Convex Optimization*. Cambridge, U.K.: Cambridge Univ. Press, 2004.

[28] Y. Huang and D. P. Palomar, "Rank-constrained separable semidefinite programming with applications to optimal beamforming," *IEEE Trans. Signal Process.*, vol. 58, no. 2, pp. 664–678, Feb. 2010.

[29] K. B. Petersen and M. S. Pedersen, "The matrix cookbook," Tech. Univ. Denmark, Kongens Lyngby, Denmark, Tech. Rep. 3274, Nov. 2012.

[30] S. Boyd, "Ellipsoid method: Notes for EE364b," Standford Univ., Stanford, CA, USA. [Online]. Available: http://stanford.edu/class/ee364b/lectures/ellipsoid_method_notes.pdf

[31] Y. Sun, P. Babu, and D. P. Palomar, "Majorization-minimization algorithms in signal processing, communications, and machine learning," *IEEE Trans. Signal Process.*, vol. 65, no. 3, pp. 794–816, Feb. 2017.

Seowoo Kang received the B.S. degree in electrical engineering from Hongik University, Seoul, South Korea, in 2012 and the M.S. degree in electrical engineering from Korea University, Seoul, in 2015, where he is currently pursuing the Ph.D. degree with the School of Electrical Engineering. In 2016, he visited the Huawei Research and Development Center, Shanghai, China, to conduct a collaborative research. His current research interests include information theory and signal processing for wireless communications, such as multiple-input multiple-output wireless network and energy harvesting communication systems. He received the Silver Best Paper Award from the IEEE Student Paper Contest in 2016.

Hoon Lee (S'14–M'18) received the B.S. and Ph.D. degrees in electrical engineering from Korea University, Seoul, South Korea, in 2012 and 2017, respectively. In 2015, he visited the Imperial College London, London, U.K., to conduct a collaborative research. In 2017, he joined Korea University as a Post-Doctoral Fellow. In 2018, he joined the Singapore University of Technology and Design, Singapore, where he was a Post-Doctoral Fellow. Since 2019, he has been with Pukyong National University, Busan, South Korea, where he is currently an Assistant Professor with the Department of Information and Communications Engineering. His research interests include machine learning and signal processing for wireless communications such as visible light communications, wireless energy transfer communication systems, and secure wireless networks.

Seokju Jang (S'15) received the B.S. and M.S. degrees in electrical engineering from Korea University, Seoul, South Korea, in 2012 and 2014, respectively, where he is currently pursuing the Ph.D. degree with the School of Electrical Engineering. In 2016, he visited the Singapore University of Technology and Design, Singapore, to conduct a collaborative research. His research interests include signal processing and optimization for wireless communications such as wireless energy transfer systems, full-duplex systems, and millimeter-wave networks.

Hanjin Kim (S'14) received the B.S. and M.S. degrees in electrical engineering from Korea University, Seoul, South Korea, in 2013 and 2015, respectively, where he is currently pursuing the Ph.D. degree with the School of Electrical Engineering. His research interests include information theory and signal processing for wireless communications such as multiple-input multiple-output wireless network and energy harvesting communication systems.

Inkyu Lee (S'92–M'95–SM'01–F'16) received the B.S. degree (Hons.) in control and instrumentation engineering from Seoul National University, Seoul, South Korea, in 1990, and the M.S. and Ph.D. degrees in electrical engineering from Stanford University, Stanford, CA, USA, in 1992 and 1995, respectively. From 1995 to 2001, he was a Technical Staff Member with Bell Laboratories, Lucent Technologies, where he was involved in high-speed wireless system designs. From 2001 to 2002, he was a Distinguished Member of Technical Staff with Agere Systems, Murray Hill, NJ, USA. In 2009, he joined the University of Southern California, Los Angeles, CA, USA, as a Visiting Professor. Since 2002, he has been with Korea University, Seoul, where he is currently a Professor with the School of Electrical Engineering. He has authored over 170 journal papers in the IEEE. He holds 30 U.S. patents granted or pending. His research interests include digital communications, signal processing, and coding techniques applied in the next-generation wireless systems. He has been elected as a Senior Member of The National Academy of Engineering in Korea (NAEK) in 2019. He received the IT Young Engineer Award from the IEEE, the Best Paper Award from APCC in 2006, the Best Research Award from the Korea Information and Communications Society in 2011, the Best Young Engineer Award from NAEK in 2013, and the Korea Engineering Award from the National Research Foundation of Korea in 2017. He was a recipient of the IEEK Joint Award in 2006, the IEEE VTC in 2009, and ISPACS in 2013. He has served as an Associate Editor for the IEEE TRANSACTIONS ON COMMUNICATIONS from 2001 to 2011, the IEEE TRANSACTIONS ON WIRELESS COMMUNICATIONS from 2007 to 2011, IEEE WIRELESS COMMUNICATIONS LETTERS from 2011 to 2013, and the IEEE ACCESS from 2016 to 2017. He was the Chief Guest Editor of the IEEE JOURNAL ON SELECTED AREAS IN COMMUNICATIONS Special Issue on 4G Wireless Systems in 2006. He is an IEEE Distinguished Lecturer.